Ambient Ion Focusing for Paper Spray Ionisation

Barry Lee Smith[1], Cedric Boisdon[1], David Romero-Perez[1], Tung-Ting Sham[1,2], Behnam Bastani[1], Yufeng Zhou[1], Stephen McWilliam[2], Abraham Kwame Badu-Tawiah[3], and Simon Maher[1]*

1) Department of Electrical Engineering and Electronics, University of Liverpool, Liverpool, L69 3GJ, UK.
2) Department of Women's and Children's Health, University of Liverpool, Liverpool, L69 3BX, UK.
3) Department of Chemistry and Biochemistry, The Ohio State University, Columbus, OH, 43210, USA.

*For correspondence and request for materials should be addressed to Dr Simon Maher, email: s.maher@liverpool.ac.uk

Abstract:

Paper Spray (PS) is an ambient ionisation technique that is conceptually simple, economical, direct and versatile. In its simplest form, the procedure for operation relies on the application of an electric potential to a triangular-shaped paper substrate with the addition of an extraction/spray solvent to generate charge droplets, without requiring any pneumatic assistance. Despite its promise and rapidly growing popularity, there are some practical challenges associated with PS implementation with scope to enhance its performance further. One such challenge relates to only a small fraction of the Taylor cone expansion being sampled at the MS inlet. In this work we propose a new arrangement for PS, which retains the inherent advantages of this popular technique without introducing additional variables, by using an ambient ion focusing lens that is held at the same potential as the paper substrate. A thorough investigation, consisting of visual spray inspection, electric field simulations and analytical evaluation, including analysis of paracetamol from saliva, shows that ambient ion focusing can provide up to 50% improvement in spray stability, 60% increase in signal intensity and a 30% improvement in detection limits for routine paper spray mass spectrometry analysis.

Introduction:

Paper spray (PS) mass spectrometry (MS) was first reported by Wang *et al*.[1] as a means for fast, qualitative and/or quantitative analysis of complex mixtures. In classic PS-MS, a porous substrate (e.g., paper) with a macroscopic sharp tip (providing a small radius of curvature) is placed under the influence of a sufficient electric potential. With the addition of an extraction/spray solvent (for wetting), analyte transport ensues followed by ionisation via a Taylor cone formation, without any pneumatic assistance. Since its introduction, PS continues to attract much research interest due to its simplicity, low cost, flexibility and wide range of potential applications,[2-10] including detection of warfare agents,[11] biomedical/biofluid analysis,[8, 12-15] toxicological screening,[16] drug testing,[17, 18] water quality testing,[19-21] aquaculture[22] and forensics analysis,[23-26] amongst many others.

Ionisation via PS is a dynamic process that is thought to occur, in general, via an electrospray-like mechanism, which can also be operated in an atmospheric pressure chemical ionisation (APCI)-like mode under certain conditions (depending mainly on the solvent system and electric field intensity).[8, 27, 28] Well-known and relatively long-standing theories have been developed that attempt to describe the electrospray process, notably the “charged residue”, “ion evaporation” and “chain ejection” models.[29-35] For a typical PS-MS experiment, when a sufficiently high DC potential is applied to the paper emitter, it is considered that excessive charge density and the surface tension of the solvent at the sharp tip of the paper, leads to the formation of a Taylor cone with an expanding jet of charged droplets. Recently it was demonstrated that the resulting ion current can be maximised when the surface energy of the substrate approaches the surface tension of the wetting solvent.[36] The precise mechanism for the formation of gas phase ions is debatable and not entirely understood. For small molecule analysis the charged residue model propounds that subsequent recursive fission of droplets due to solvent evaporation and intra-droplet Coulombic forces produce a fine spray plume of charged droplets and ions, collectively referred to as charged particles.[37] These are accelerated under the influence of the electric field gradient towards the MS inlet (serving as a counter electrode).

Regardless of ionisation efficiency, (which, for electrospray, can be high, particularly for low flow rates and low concentrations[38]) it has been shown that even for commercial electrospray ionisation (ESI)-MS interfaces, the ion transmission efficiency (also known as the ion sampling efficiency) from the atmospheric pressure environment to the first stage of the mass spectrometer is low (typically < ~20 %).[39, 40] The expansion of the droplet plume for electrospray-type ionisation sources, such as PS, leads to only a small fraction of the charged particles being sampled at the atmospheric pressure interface (API).[41] This is a source of significant sample loss, as the outer cross-sectional area of a typical PS plume is several times greater (typically, ~20-30x) than that of an MS inlet capillary (Fig. 2).

Desolvation also plays a key role in gas phase ion generation.[42] Ineffective desolvation leads to the transmission of clusters and/or droplets, as opposed to gas phase ions, into the mass spectrometer. Therefore, as is often the case, even for commercial ESI sources, spray plume sampling is usually carried out at the edge of the Taylor cone expansion where fine droplets are more prominent.[43] Nanoelectrospray ionisation (nESI) offers more efficient desolvation, with initial droplet sizes around an order of magnitude smaller (~200 – 300 nm)[44, 45] . Many strategies have been utilised to aid desolvation and overall effectiveness for conventional ESI, including (but not limited to): using a heated capillary transfer tube[46] or heated gas flow (e.g., nitrogen),[47, 48] off-axis positioning of the emission tip to enable nebuliser assisted sampling of finer droplets by the MS inlet capillary,[49]

orthogonal sampling of the spray plume (especially for higher solution flow rates),[50] electrostatic ion focusing[51] and inertial sorting,[52] amongst others.

Such challenges are even more pertinent for PS-MS, being a substrate-based ambient ionisation technique.[53] For a typical PS setup, the mean droplet size is usually in the region of ~1-2 μm[27]. The key advantages of PS relate primarily to the properties and benefits derived from the paper substrate (e.g., low-cost; widely available; convenient sample collection, storage and transport; wicking capacity; biodegradable; lightweight; functionalisable, etc.), which enables sampling, separation and ionisation to be achieved on the paper. Moreover, in line with the principles of ambient ionisation, PS-MS requires no (or minimal) sample preparation and analyses can be completed within short timeframes (e.g., < 1 min is typical, from sampling to result). Any new strategies to enhance PS operation and performance should not detract from its signature benefits. Since its relatively recent inception there have been a number of studies that have contributed to the advancement of the PS technique in terms of interfacing with a mass spectrometer such as: characterising the tolerance of the PS emission tip positioning relative to the MS inlet,[54] a high throughput PS platform,[55] PS mounting system with integrated solid phase extraction[56] and 3D printed cartridge systems[57, 58], amongst others. Interestingly, Salentijn *et al.*[57] briefly investigated the effect of a focusing electrode as part of their cartridge design which showed promise, but they encountered difficulties in generating electrospray at increased electrode potentials (max. electrode potential possible was ~30% of the applied substrate potential).

In this work we propose a simple and effective method for increasing the magnitude and stability of the ion signal for PS-MS that can be readily implemented with minimal complexity. We reasoned that an ambient ion lens can be used to accomplish this goal by forming a more focused and collimated beam of charged particles. We set about testing this approach with the proviso that the implementation should not diminish from the benefits afforded by conventional PS-MS. This is achieved by means of a ring-shaped focusing electrode placed between the apex of the PS substrate and the inlet of a mass spectrometer. Moreover, the same voltage is applied to both the paper substrate and the focusing electrode so as to preserve the simplicity of operation (without introducing additional variables). The impact of the electric field generated by the focusing electrode was investigated and, as expected, is shown to transform the diverging conical profile of the spray plume into a focused collimated beam (with minimal divergence), directing an increased charge density to the mass spectrometer inlet with reduced signal variance. A thorough investigation is carried out to demonstrate applicability to mass spectrometry analysis comparing this approach against a typical/conventional paper spray setup for the analysis of paracetamol from saliva.

Methods

Ring Lens (RL)-PS-MS Interface

To achieve concentricity and repeatable positioning of the RL in relation to the MS inlet, a 3D printed structure was designed to hold the RL at a fixed distance from the entrance orifice. Fig. 1 shows a CAD render of the designed structure and the important physical dimensions of the experiment. The component labels refer to: (1) Waters Xevo TQ-MS sampling cone assembly, (2) 3D printed RL holder, (3) RL and (4) Paper spray substrate. The dimensions of the RL used in all experiments: 20.5 mm diameter and 3 mm thickness, with the central plane of the RL fixed 10.5 mm from the entrance orifice. The paper triangle protrudes though the RL by 2 mm (unless stated otherwise). For experiments operating below 5000 V the internal MS power supply was used to provide the spray voltage to the paper substrate. When a spray voltage > 5000 V was required, an external HV PSU (Leybold, UK) was used. The position of the paper substrate in relation to the RL was adjusted via micro-meter adjustment (x, y and z linear stages) until concentrically located within the ring lens. For standard PS experiments, the RL assembly was removed, otherwise the experimental configuration remained the same.

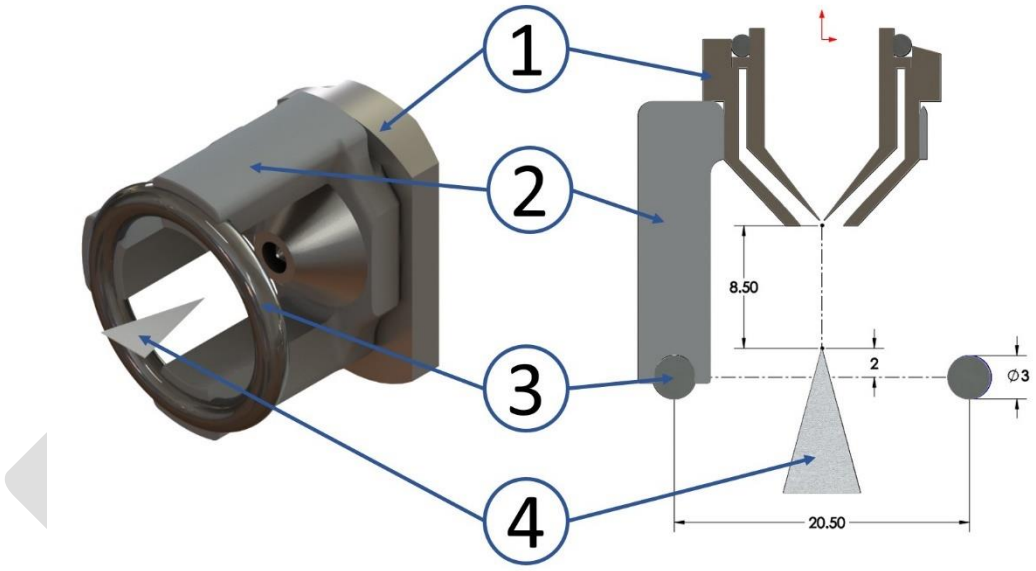

Figure 1: *CAD render of: (1) Sampling cone assembly, (2) 3D printed RL holder, (3) RL and (4) Paper spray substrate and the relative distances between components. All units are in mm unless otherwise stated.*

Automated PS/RL-PS Method

To facilitate rapid data collection, a syringe driver (KDS Scientific, USA) was programmed to deliver automated spray solvent dosing to the paper substrate in conjunction with applying the spray voltage. At the start of each experiment, an initial dose volume of 10 µL was delivered to the paper surface via a peek capillary (I.D. 100 µm) suspended ~2 mm above the surface of the paper with the other end connected to a syringe through a union fitting. After a delay of 10 seconds a further 5 doses of 10 µL were programmed to be delivered at the same time as the spray voltage was on to guarantee an excess of solvent throughout the spraying period. The spray volume was delivered over a 40 second period with 20 second off time between doses. The syringe pump driver also controlled the application of the spray voltage via a digital output signal connected to a solenoid valve mounted in front of the safety interlock microswitch on the MS front panel (Waters Xevo TQ-MS). When activated, the solenoid valve enables the application of the voltage from the internal MS HV supply connected to the

crocodile clip holding and electrically connecting the paper spray substrate. The magnitude of the applied voltage is set prior to the experiment commencing via the MS tune page (capillary voltage setting) in MassLynx software. For all PS and RL-PS experiments, the spray voltage was set to 3700 V and 5000 V unless otherwise stated. The equivalence of these voltages in terms of the field generated is noted in the electric field simulation results section.

Mass Spectrometry Settings

All RL-PS and PS experiments were performed on a Waters Xevo TQ-MS triple quadrupole mass spectrometer in positive ionisation mode. The ion source temperature was maintained at 70°C (in part to avoid outgassing and melting of the 3D printed resin material of the RL holder). Quantitation was performed using multiple reaction monitoring (MRM). The following transitions were monitored: *m/z* 152 → 110 for paracetamol and *m/z* 156 → 114 for paracetamol-D4 acting as the internal standard (IS), respectively, with a dwell time of 0.1 s per transition. The cone voltage and collision energy were set to 20 V and 20 eV, respectively. The MS instrument was controlled by using Waters MassLynx software (version 4.1, MA, USA). No further optimisations were performed and any remaining instrument settings were set as per the manufacturer's recommendation.

Chemicals and reagents

Paracetamol (purity ≥ 98%) and reagent-grade formic acid (≥ 95%) were purchased from Sigma–Aldrich (St. Louis, Mo, USA). Isotopically labelled paracetamol-D4 solution (100 µg/mL in methanol) was obtained from Cerilliant (Round Rock, TX, USA). Methanol (99.8%, HPLC grade) was purchased from Fisher Scientific (Loughborough, UK). Distilled water was supplied by ReAgent Chemical Services (Cheshire, UK). Chromatography paper (25mm, Grade 1) was purchased from Whatman (Maidstone, UK).

Preparation of stock and calibration solutions

A standard stock solution of paracetamol (10 mg/mL) was prepared with methanol and stored at -20 °C. 20 µg/mL and 1 µg/mL diluted standard solutions were further diluted to prepare working solutions of paracetamol at 1-15 µg/mL and 0.1-0.8 µg/mL with distilled water, respectively. Nine calibration standard solutions were prepared at concentrations of 0.36, 0.54, 0.72, 0.9, 1.8, 4.5 µg/mL by mixing 180 µL of each working solution with 20 µL internal standard (IS), acetaminophen-D4 (10 µg/mL). A blank solution with spiked IS was prepared using distilled water to replace the standard solution. All solutions were stored in a refrigerator at 2-8°C before analysis.

Saliva samples

Saliva from a single source was centrifuged at 3000 rpm for 5 minutes at room temperature. 100 µL supernatant was mixed with 300 µL methanol and vortexed for 30 seconds. The mixture was allowed to stand in the freezer for 30 minutes for deproteination, followed by a further centrifuge at 3000 rpm for 5 minutes. 180 µL diluted saliva supernatant was spiked with 20 µL IS followed by vortex mixing for 30 seconds. The dilution factor of the saliva was 4.4.

Paper spray sample preparation

Paper substrates were cut into a triangular shape with scissors. The paper surface area was 64 mm^2 (base 8 mm, height 16 mm). The spray solution was prepared as 50% methanol in distilled water with 1% formic acid. 15 µL of calibration solutions, blank solution and diluted saliva samples were pipetted onto the scissor-cut paper and allowed to dry in ambient conditions for at least 15 minutes before PS-MS analysis.

Data analysis

Data acquisition was performed using Waters Masslynx software (version 4.1). MSConvert software converts the .RAW waters files to .mzML file format for importing the raw chromatogram data into Matlab (Mathworks, USA) for analysis and visualisation. Each file contains 2 chromatograms containing 5 sprays for every concentration. The start and end scan indexes for all sprays in each chromatogram are automatically identified using findchangepts() function and the area under the curve between the time indexes is calculated using trapezoidal numerical integration via the trapz() function. The peak area ratio is then calculated by dividing the paracetamol transition *m/z* 152 → *m/z* 110 peak area by the IS transition *m/z* 156 → *m/z* 114 peak area. Finally, the ratio means, standard deviations and relative standard deviations (RSDs) are tabulated for producing linear regressed calibration curves.

Simion Field Simulations

Electric field simulations were carried out using SIMION 8.1 (Scientific Instrument Services, NJ, USA). Briefly, a geometry file was coded to produce the required 3D geometry with and without the ring lens. A potential array with 0.05 mm resolution across a 15 mm x 11 mm x 11 mm workspace domain was created. Planar symmetry was employed in the *y* and *z* dimensions to limit the array memory allocation and decrease simulation time. A user program performed the voltage sweep and electric potential assignment to the relevant electrodes in addition to generating an appropriately labelled text file containing the electric field vector components for *x*, *y* and *z* for each grid unit at every simulated voltage. The exported text files were then imported into Matlab for visualisation and comparison. For particle tracing simulations the SDS collision model[59] user program was applied to the workbench to simulate trajectories at atmospheric pressure. Initial ion conditions were constant in both RL-PS and PS simulations and were as follows: (1) Distance from triangle tip: 1mm. (2) Initial beam diameter: 2mm filled circle distribution. (3) Mass: 28amu. (4) Charge: +1.

Results

Ring Lens and Paper Spray Visual Inspection and Simulation

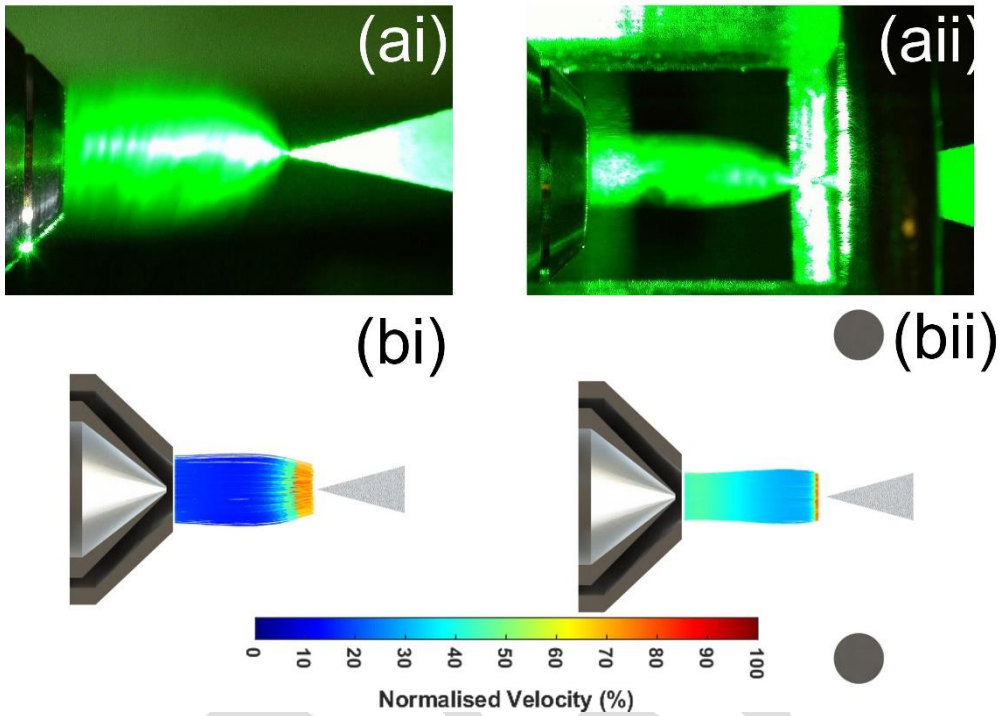

Figure 2: *Visual comparison of Spray profiles for: (ai) PS and (aii) RL-PS; Images (bi) PS and (bii) RL-PS are particle tracing simulations at atmospheric pressure using Simion with SDS collision model, where coloured traces relate to axial particle velocity (normalised).*

An image showing spray formation from PS is presented in Fig. 2 (ai) under typical spray conditions (50% methanol in water, +3500 V). A conventional PS plume with widely dispersed droplets emerging from the paper tip is illuminated by a wide angled laser diode. The relative diameter of the spray plume in comparison to the MS API (shown on the left of the image, Fig. 2 ai) emphasises, by visual inspection, the low sample transfer efficiency during PS experiments (also illustrated in Fig. S1c, supplementary information). In contrast, Fig. 2 (aii) shows the spray formation when performing PS with a RL electrode located between the paper tip and the MS-API. Using a typical spray solvent of 50% methanol in water, spray voltage of 5000 V with corresponding ring lens voltage also at 5000 V, this produces a narrow, collimated spray plume. An elevated spray voltage (5000 V for RL compared to 3500 V for classical PS) is necessary to initiate a RL-PS plume due to a reduction in the electric field strength at the apex of the paper triangle because of the presence of the equipotential RL (as discussed further in the electric field simulations section). The distance between the inlet to paper apex was approximately 8 mm with the front plane of the ring a further 0.5 mm from paper apex. These images are also supported by particle trajectory traces simulated with Simion as shown in Fig. 2 (b). Fig. 2 (bi) represents the conventional case with 3500 V applied to a triangular electrode (representing the PS substrate) with 30 V applied to the MS inlet cone and Fig. 2 (bii) includes the addition of the ring lens which is held at 5000 V along with the triangular electrode. The degree of agreement between trajectory plots to live spray imagery is notable given the model simulates movement of individual charge particles whereas clearly macro-droplets are present in Fig. 2(ai) and 2(aii), nevertheless the similarity and focussing effect due to the presence of the ring electrode is evident. In addition to the radially confined beam diameter, particle trajectory streamlines are colour mapped to the normalised

axial velocity (x direction; as per the co-ordinate system used in Fig. 3) indicating ~146% increase in mean velocity for RL-PS over PS. Further visual investigation of the spray plumes from different spray events are shown in Fig. S1 (supporting information), which also depicts high resolution, magnified, pseudo-colour images mapped to the droplet density, illustrating the effect of the RL on the spray plume if multi-jet[27] spraying occurs. Moreover, further reductions in spray diameter can be observed when the voltage is increased to 8000 V and the paper substrate is repositioned such that RL is between the paper substrate and MS inlet (supporting information Fig. S1 (cii)). Note, this configuration requires use of an external high voltage power supply which can expose the MS to voltages potentially beyond its tolerance rating.

Electric Field Simulations

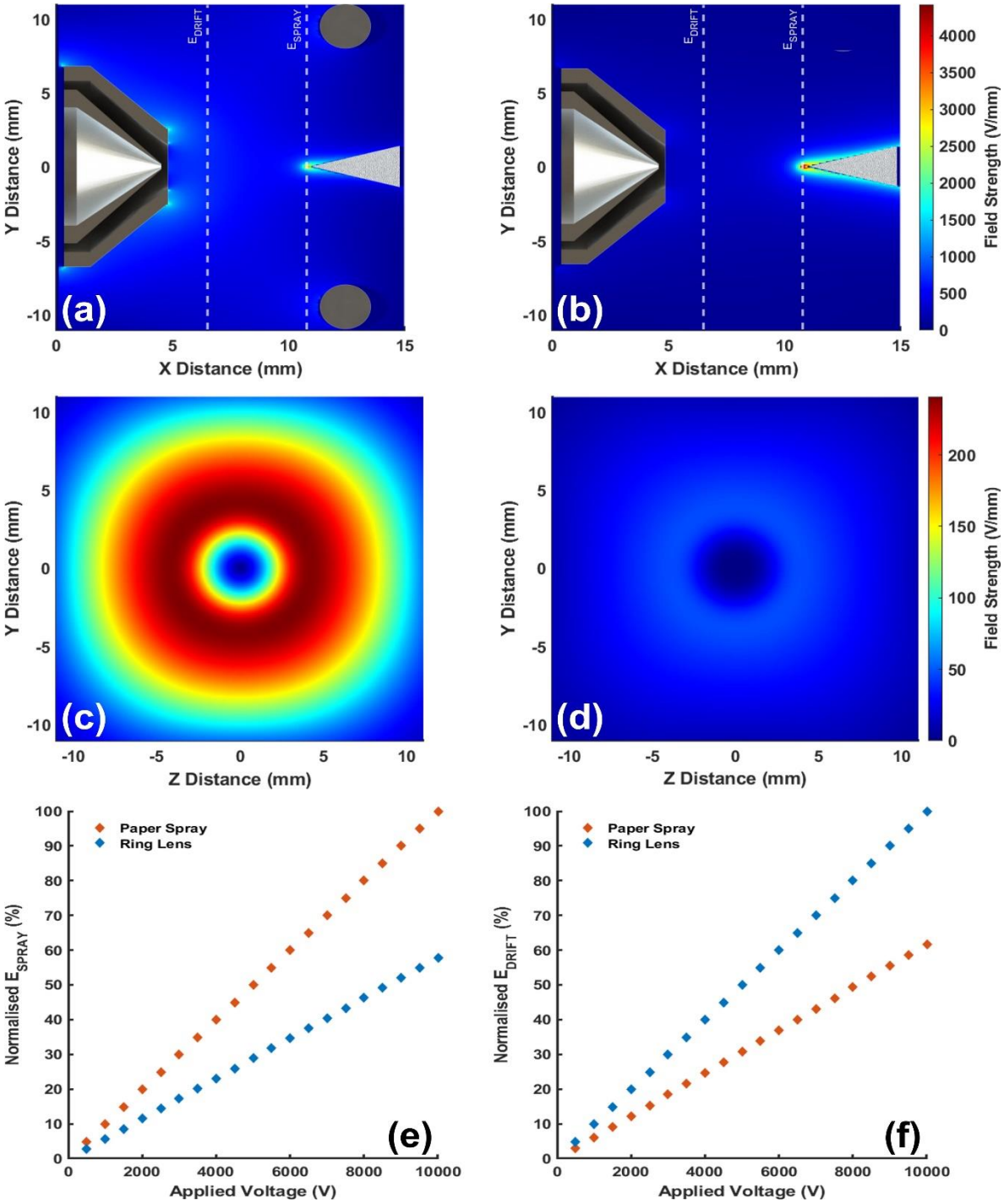

Figure 3: *Simion simulation field plotting results for: (a) Field vector magnitude in x-y plane for RL-PS, (b) Field vector magnitude in x-y plane for conventional PS (i.e., without RL), (c) Field vector magnitude in y-z plane at E_{drift} for RL-PS, (d) Field vector magnitude in y-z plane at E_{drift} for conventional PS, (e) Field vector magnitude at E_{spray} for spray voltages 500 V to 10,000 V for RL-PS and conventional PS, (f) Field vector magnitude at E_{drift} for spray voltages 500 V to 10,000 V for RL-PS and conventional PS.*

Electric field strength plots generated in Simion, using the exact geometric parameters of the RL and PS experiments (Fig. 1), are shown in Figs. 3(a) and (b) for RL-PS and PS, respectively. As is to be expected, the largest field magnitude is located at the emission tip where a spray voltage of 5000 V is applied to the substrate and RL in Fig. 3a, and 3500 V is applied to the classic PS setup in Fig. 3b. The

MS inlet is grounded in both cases. There are two regions of particular interest with regards to field analysis for examination of the RL effect on PS experiments. (1) At the tip of the paper substrate where charged droplets are generated we have the spray formation field (E_{spray}). (2) The other region of interest is in the region between the emission apex and the MS inlet, where we have the drift field (E_{drift}). To aid the discussion, these regions, E_{spray} and E_{drift}, are defined in (a) and (b), where E_{spray} is a plane located at (10.8, *y*, *z*) [mm] and E_{drift} is a plane located at (6.5, *y*, *z*) [mm] at a distance of 4.5 mm from the triangle apex (n.b., the origin of this Cartesian coordinate system is located on the inside of the sampling cone along its central axis, as can be seen in Fig. 3). The Electric field strength cross-section at E_{drift} is plotted in Figs. 3(c) and (d) for the same applied potentials as (a) and (b), respectively. Here the field plots exhibit stark differences between the electric field forces that would be experienced by the charges. Large (>200 Vmm^{-1}) radially inward forces generated by the potential applied to the RL result in a narrow corridor in which the ions are compelled to travel towards the inlet (as demonstrated in Fig. 2(aii)). In the absence of a ring lens (Fig. 3(d)), the focusing field magnitude is significantly reduced (<50 Vmm^{-1}) as would be expected during a typical Taylor cone formation with PS, as seen in Fig. 2(ai).

To produce a meaningful comparison between classic PS and RL-PS, despite the differences in applied voltage, a constant value for E_{spray} at the substrate apex can be used. It is reasonable to assume, for the same solvent system (and solvent surface tension), analyte concentration, solution conductivity and electric field strength at the apex of the triangle (i.e., the factors dictating the spray formation), a similar ionic current will be ejected from the paper emitter. Fig. 3(e) shows a plot of the normalised electric field magnitude at the apex of the paper substrate for a voltage sweep from 500 V to 10,000 V applied to the RL and PS setups. From this we can derive the equivalent voltage that equates the fields at the tip for both setups. For example (as plotted in Fig. 3 (a), (b), (c) and (d)), 3500 V applied to the classic PS setup has an equivalent field magnitude when approximately 5000 V is applied to the RL setup. However, the effect on E_{drift} when operating at higher spray voltages is to increase E_{drift} from 12% to 52% of the maximum simulated E_{drift} as derived from Fig. 3(f). We expect that this increase has two key effects on ambient ion transportation: (1) a focusing effect, as previously noted, and, (2) a substantial rise in the *x* component of the field vector leading to an increased ion velocity since drift velocity is proportional to the applied voltage (Fig. 2 (b)). An increase in velocity can have implications for the internal ion energy and possible fragmentation of fragile molecules but further investigation is required (e.g., survival yield experiments to determine the internal energy distribution[1]). The positive effects on transmission likely emanate from the reduced time the ion spends at atmospheric pressure incurring fewer loses, and increased friction between the ions and background gases along with an increase in inter-charge forces which may aid desolvation and ion evaporation. Further ion modelling based on direct charge-charge interactions is the subject of ongoing research.[60-62] The overall effect of the RL is to effectively decouple E_{drift} from E_{spray}. Almost any E_{drift} can be established whilst setting an E_{spray} that generates a stable spray by varying the geometric parameters of the RL and relative positioning of the RL, paper spray substrate and grounded inlet.

Experimental confirmation of increased ion transmission for equivalent E_{spray} is determined by mass spectral analysis of 20 ppm paracetamol dried onto a paper substrate and subsequently sprayed into the MS using a spray solvent of 50% methanol in water with 1% formic acid. The following applied voltages were derived from the simulation results (Fig. 3(e)) to yield an equivalent E_{spray} field: 3000 V, 3500 V, 4000 V and 5000 V, 6000 V, 7000 V for PS and RL-PS, respectively. These were applied to the paper substrate with constant distances maintained between paper tip and MS inlet. Concentricity and accurate linear distance between the ring lens and the MS inlet are guaranteed by using a 3D printed mount installed on the inlet cone to hold the RL. The experimental set up can be seen in the methods section (Fig. 1); a .STL design file for mounting a 23.5mm outer diameter ring at a distance of 8.5 mm from the entrance orifice of the MS is included along with the supplementary information. Fig. 4(a) shows the raw intensity measurement of the paracetamol fragment ion *m/z* 110 after collision induced dissociation (CID) of the paracetamol parent ion at *m/z* 152. A substantial increase in ion intensity is recorded for each equivalent E_{spray} field, 2.6 x 10^6 counts vs 1.3 x 10^6 counts; 3.1 x 10^6 counts vs 1.6 x 10^6 counts and 4.0 x 10^6 counts vs 7.4 x 10^5 counts, for PS:RL-PS spray voltages 3000:5000 V, 3500:6000 V and 4000:7000 V. This was further supported by monitoring the total ion current with an ambient Faraday detector array[63] along with corresponding simulations (Fig. S2, supporting information). The measurement of raw spray stability also exhibited a noticeable decrease in variance for RL-PS from an average across 5 replicate measurements from 3 experiments of ~21% for classical PS to ~11% for RL-PS as seen in Fig. 4(b).

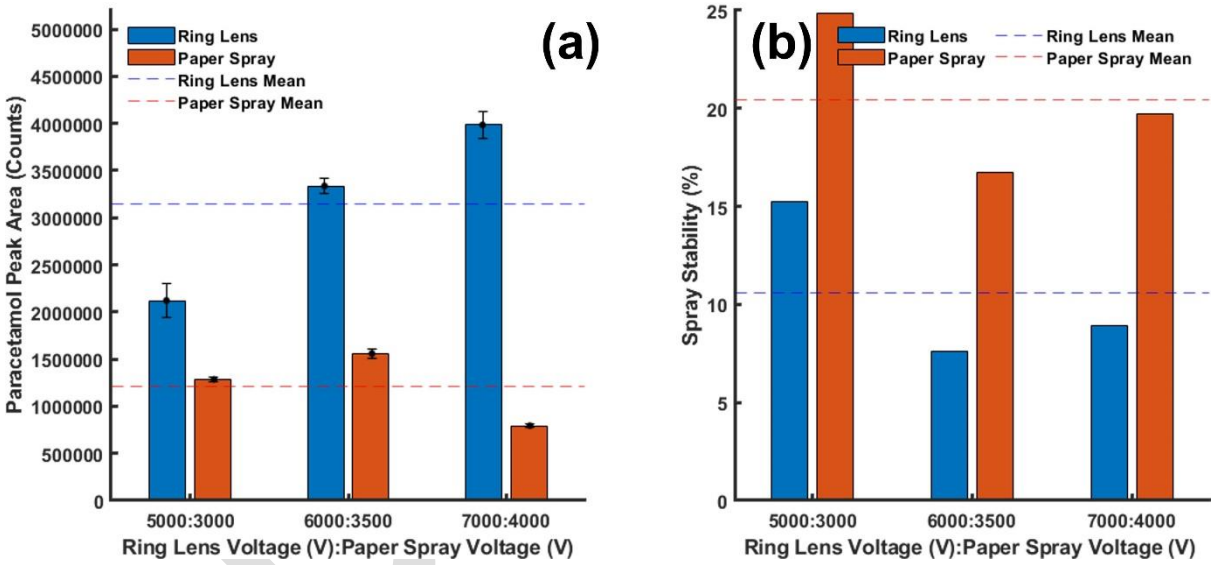

Figure 4: *(a) Comparison of integrated peak area intensity for paracetamol product ion (m/z 110) by CID from paracetamol precursor ion (m/z 152) for RL-PS (blue) and PS (red) at spray voltages 5000 V: 3000 V, 6000 V: 3500 V and 7000 V: 4000 V for PS and RL-PS, respectively. (b) Comparison of the paracetamol product ion (m/z 110) peak height stability for all replicates for RL-PS (blue) and PS (red) at spray voltages 3000 V, 3500 V, 4000 V, and 5000 V, 6000 V, 7000 V for PS and RL-PS, respectively. Dashed lines correspond to the mean of all readings for RL-PS and PS.*

The comparison of measurements taken at equivalent E_{spray} fields shows a distinct enhancement of RL-PS versus PS (Fig. 4). However, this doesn't exclude the possibility that an optimised PS arrangement can lead to an increase in signal intensity relative to RL-PS. One parameter that is important in this regard is the paper tip to inlet distance. Therefore, a series of further experiments gauging the effect of distance between paper apex and MS inlet on RL-PS and PS performance were conducted (Fig. 5). RL-PS outperformed PS for every measured distance: 4 mm: 1.30 x 10^9 vs 1.14 x 10^9 counts; 5 mm: 2.16 x 10^9 vs 1.02 x 10^9 counts; 6 mm: 3.16 x 10^9 vs 9.45 x 10^8 counts; 7 mm: 3.60 x

10^9 vs 1.21 x 10^9 counts; 8mm: 2.87 x 10^9 vs 6.70 x 10^8 counts; 9 mm: 1.55 x 10^9 vs 5.61 x 10^8 counts (Fig. 5(a)). The signal intensity difference was minimal when the paper was positioned at 4mm distance from the inlet likely due to the substantial protrusion of the paper through the plane of the ring lens reducing the focussing effect. Distances greater than 4mm resulted in approximately two to three times improvement in the signal intensity of the ion at *m/z* 152 corresponding to the paracetamol precursor peak. Images of the paper position relative to MS inlet are shown in the supporting information (Fig. S4) along with the raw single ion chromatograms of the precursor peak for each corresponding distance. RSDs of replicate measurements for each paper apex to MS inlet distance are shown in Figure 5(b) where RL-PS demonstrates increased signal stability at each distance with overall mean RSDs of 6.7% and 17.2% for RL-PS and PS, respectively. Further examination of the full scan mass spectra shows a reduction in background ion intensity for RL-PS, suggesting a minor improvement in desolvation (supporting information Fig. S5).

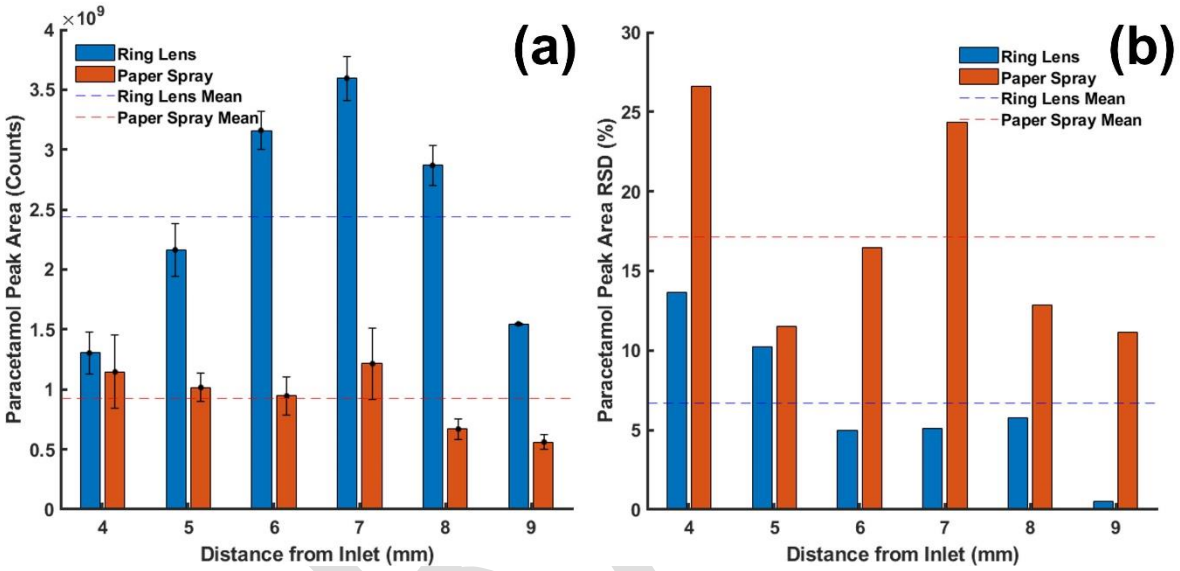

Figure 5: *(a) Comparison of integrated peak area intensity for paracetamol precursor ion (m/z 152) for RL-PS (blue) and PS (red) at paper tip to MS inlet distances of 4 mm, 5 mm, 6 mm, 7 mm, 8 mm, and 9 mm. (b) Comparison of the relative standard deviation (RSD) of the paracetamol precursor ion (m/z 152) peak area for replicates of RL-PS (blue) and PS (red) at paper tip to MS inlet distances of 4 mm, 5 mm, 6 mm, 7 mm, 8 mm, and 9 mm. Dashed lines correspond to the mean of all readings for RL-PS and PS. The corresponding raw data is provided in the supplementary information (Fig. S4).*

Analysis of Paracetamol in Saliva by RL-PS

RL-PS Calibration Curve

Evaluating RL-PS performance for routine, automated MS analysis is achieved through the generation of a calibration curve and analysis of paracetamol spiked in saliva at 1000 ng/mL. A calibration curve was prepared ranging from 360 ng/mL to 4500 ng/mL (Fig. 6). Each concentration measurement is the ratio of integrated peak area of the main paracetamol fragment ion *m/z* 110 to integrated peak area of the IS, paracetamol-D4 fragment (*m/z* 114). Each measurement was subjected to 5 repeat sprays; the mean and standard deviation are shown in Fig. 6 along with a regressed linear fit line. Examination of the coefficient of determination yielded an almost perfect fit to the data of 0.999 and RSDs of 3.79%, 1.25%, 1.30% 1.72%, 1.91% 0.99% for the following concentrations 360 ng/ml, 540 ng/ml, 720 ng/ml, 900 ng/ml, 1800 ng/ml and 4500 ng/ml, respectively. To facilitate automated data collection, the RL-PS spray voltage was restricted to a sub-optimal 5000 V due to the maximum output voltage of the internal MS high voltage power supply (the maximum of which is 5000 V). This, in conjunction with a

programmable syringe driver, which delivers coordinated solvent dosing and spray voltage application to the paper substrate without manual intervention (see method section, Automated PS/RL-PS Method).

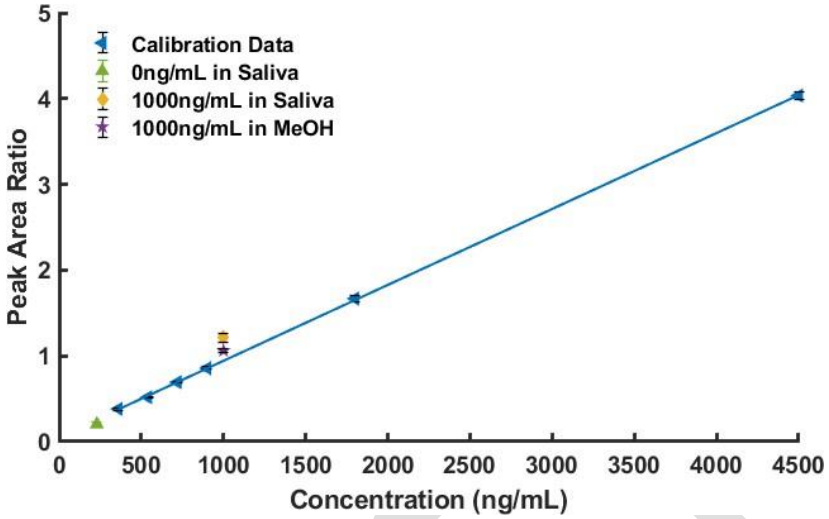

Figure 6: *Calibration curve for paracetamol fragment m/z 110 : internal standard fragment m/z 114 peak area ratio. Also included are data for 1000 ng/mL of paracetamol spiked into raw saliva and methanol.*

Saliva Analysis

Saliva spiked with 1000 ng/mL paracetamol and internal standard in addition to a blank containing only internal standard were directly sprayed from paper after minimal sample preparation (centrifugation followed by a simple protein denaturisation, as outlined in the methods section including methanol dilution by a factor of 4.4). The ratio measurement was compared with the same concentration of paracetamol prepared in methanol to determine the effect of the complex saliva matrix on the spectral response (Figure 6). Sample recovery from 1000 ng/mL of paracetamol doped in saliva was 114.2% of the response observed from spiking in methanol. The spray stability of the 5 repeats (supplementary information Figs. S6 (b) & (c) are noticeably subject to increased variance relative to the calibration curve and this is most likely due to chemical noise from the matrix containing interferents. The RSD for peak area ratio measurement was 4.65%, 1.81% for the saliva sample and methanol sample respectively, and the signal intensity exhibited an almost 10-fold reduction. It is worth noting that the 1000 ng/mL examined here is below the expected therapeutic range for paracetamol in saliva (5-20 mg/mL)[64]. A further experiment whereby direct spray of spiked saliva prior to any sample preparation was attempted, but due to matrix interference, no significant signal for paracetamol or IS was detected. One-step direct analysis of salivary analytes with PS is the subject of ongoing work.

Comparison of RL-PS with Classical PS

Classic PS Calibration Curve

A further calibration curve employing conventional PS to deduce inter-method performance was prepared and is shown in supplementary information Fig. S7. For the PS calibration curve, the same concentrations were analysed as for RL-PS and a similarly excellent fit of 0.999 was obtained with RSDs of 2.64%, 1.05%, 0.79% 3.01%, 1.50% 2.72% for concentrations 360 ng/ml, 540 ng/ml, 720 ng/ml, 900 ng/ml, 1800 ng/ml and 4500 ng/ml, respectively. Fig. 7(a) shows the RSD comparison with RL-PS yielding an average RSD of 1.82% compared to 1.95% for classic PS. The raw chromatograms for both RL-PS and PS can be seen in the supplementary information (Fig. S8) where the scan indexes used to

calculate area under the curve are highlighted by the blue (RL-PS) and red (PS) shaded regions, in Fig. S8 (a) and (b) respectively.

Limits of Detection

The limits of detection and quantification (LOD and LOQ) were calculated as per equations (1) and (2):

$$LOD = \frac{3\sigma}{s} \quad (1)$$

$$LOQ = \frac{10\sigma}{s} \quad (2)$$

Where σ and s are the standard deviation of the response and the slope of the calibration curve respectively. For RL-PS, they are lower than conventional PS by 34.4% (61 ng/mL vs 93 ng/mL; 202 ng/mL vs 309 ng/mL). The saliva measurement spiked with only the internal standard at 1000 ng/mL (supplementary Fig S6(a)) was determined to be 229 ng/ml, but it is significantly below the therapeutic range for paracetamol in saliva. This background measurement is likely due to matrix interference from saliva (such as isobars in the saliva matrix sharing the same *m/z* as paracetamol).

Accuracy

Accuracy (relative bias, %) of each method is evaluated by measuring the distance of each replicate to the calibration fit line as defined in equation (1):

$$Accuracy\ (\%) = \frac{|Calculated\ Concentration - Theoretical\ Concentraion|}{Theoretical\ Concentration} \times 100 \quad (1)$$

The mean and spread of the accuracy for each concentration is as follows (Fig. 7(b)): RL-PS: 3.2% ± 1.8%, 3.5% ± 1.1%, 1.0% ± 0.7%, 1.2% ± 1.0%, 1.6% ± 1.1%, 0.7% ± 0.5%. PS: 5.5% ± 2.2%, 4.4% ± 0.9%, 1.3% ± 0.7%, 2.1% ± 1.6%, 5.2% ± 1.4%, 3.3% ± 2.8%. Both methods demonstrated excellent accuracy and, on average, RL-PS yielded a 2-fold improvement over classic PS (1.8% v 3.6%). Generally one might expect that accuracy should improve as the concentration of analyte in the spray increases, however our findings exhibit some variability in this regard as indicated by the error bars. This is not unexpected for ambient ionisation experiments (subject to external environmental factors) and in particular PS as variation amongst paper substrates is to be expected. Nevertheless, the reported accuracy for both methods are well within acceptable analytical standards[65].

Spray Plume Sampling Efficiency

Fig. 7(c) shows the raw measure of the IS chromatogram peak height and is utilised to determine the sampling efficiency since the IS is consistently applied in the same concentration for each method. The average measurement across all data points resulted in 71% higher peak heights (65000 counts vs 38000 counts) in the case of RL-PS over PS. The additional recovery of the 1 ppm spiked IS further demonstrates increased charged density (see also Fig. S2, supplementary information) of the narrower spray leading to a higher intake of analyte ions into the MS. The intensity counts for each concentration in Fig. 7(c) are 19,000 vs 65,000 counts; 67,000 vs 45,000 counts; 79,000 vs 37,000 counts; 67,000 vs 40,000 counts; 52,000 vs 16000 counts; and, 100,000 vs 24,000 counts for RL-PS and PS, respectively. RL-PS outperforms PS in all except one experiment (360 ng/ml). We believe this to be an outlier that is possibly a consequence of misalignment when positioning the paper substrate in the crocodile clip with respect to the central axis of the RL. In future work this effect could be mitigated by the inclusion of a simple structure to prevent any sagging of the paper and therefore prevent misalignment of the paper substrate in this dimension.

Spray Stability

The variability of the IS peak height measurement is 30.96% vs 14.64%, 9.71% vs 16.68%, 16.17% vs 24.08%, 13.14% vs 17.99%, 15.83% vs 18.38%, 18.83% vs 33.13% for RL-PS and PS, respectively, for each concentration (Fig. 7(d)). The mean spray RSD is 17.4% for RL-PS and 20.8% for classic PS (Fig. 7(d)). Overall, the spray stability result is very good for both methods. Spray stability is influenced by several factors: (1) Instrument scan time of 0.1 scans per second will ultimately have introduced variance into the measurement but the requirement to take near instantaneous measurements of analyte and internal standard is the higher priority. (2) Paper preparation process: a cutting guide template was used to best ensure a standardised paper size and macro-tip sharpness, but it is likely to be a source of variance. To the best of our knowledge a systematic investigation of paper cutting methods for PS has not been carried out. (3) Positional variability between the paper and MS inlet when reloading with different paper substrates.

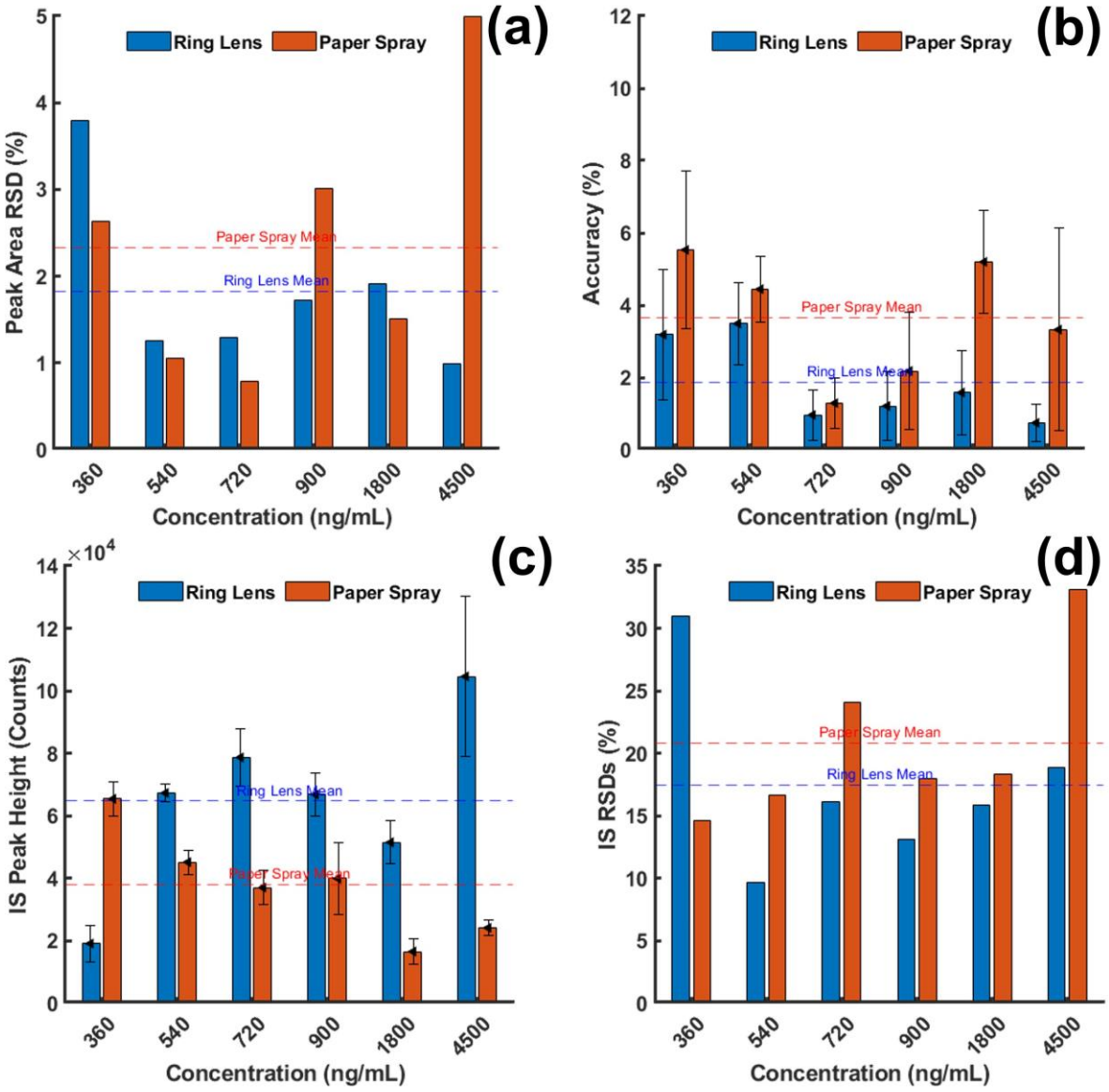

Figure 7: *Key metric comparisons between RL-PS and PS. (a) Peak area measurement RSD, (b) Replicate accuracy, (c) IS peak height and (d) IS spray stability.*

Conclusions

PS is an ambient ionisation technique that continues to attract much attention due to its many advantageous characteristics. Nonetheless, conventional PS in a typical setup requires a Taylor cone formation which can exhibit erratic behaviour, due to the nature of the substrate, and large divergence due to Coulombic expansion leading to significant ion current loss at the MS inlet. The ambient ring lens arrangement demonstrated herein provides a simple means to produce a stable and collimated beam profile, as demonstrated with paracetamol analysis from saliva (without introducing additional operation parameters). The net result is an improved performance in terms of accuracy, detection limits as well as increased ion current density and overall spray stability. This work opens up a number of possible avenues for further improvements and investigations. For instance, with the ring lens and base of the paper substrate held at the same electric potential, one could reasonably expect that the migration forces associated with capillary action should dominate since the effective electric field on the paper substrate itself is negligibly small (i.e., it may be possible to perform classic paper chromatography *in-situ* with paper spray analysis in a one-step process). Furthermore, the ring lens approach can aid investigations relating to the distance of droplet travel under ambient conditions. Since the plume is effectively collimated and the sampling efficiency is improved it would be interesting to examine the distance effect (at increased distances) which can benefit charged droplet reaction acceleration experiments.[66] Finally, since E_{drift} can be effectively decoupled from E_{spray}, the influence of the RL on the axial velocity of charged particles has some interesting connotations; further investigation and optimisation with a wider range of analytes is required to understand the potential influence on ambient declustering, desolvation and fragmentation.

References

[1] H. Wang, J. Liu, R.G. Cooks, Z. Ouyang, Paper spray for direct analysis of complex mixtures using mass spectrometry, Angewandte Chemie International Edition, 49 (2010) 877-880.
[2] L.C.d. Silva, I. Pereira, T.C.d. Carvalho, J.F. Allochio Filho, W. Romão, B. Gontijo Vaz, Paper spray ionization and portable mass spectrometers: a review, Analytical Methods, 11 (2019) 999-1013.
[3] C.-H. Lin, W.-C. Liao, H.-K. Chen, T.-Y. Kuo, Paper spray-MS for bioanalysis, Bioanalysis, 6 (2014) 199-208.
[4] N.E. Manicke, B.J. Bills, C. Zhang, Analysis of biofluids by paper spray MS: advances and challenges, Bioanalysis, 8 (2016) 589-606.
[5] B.S. Frey, D.E. Damon, A.K. Badu-Tawiah, Emerging trends in paper spray mass spectrometry: Microsampling, storage, direct analysis, and applications, Mass Spectrometry Reviews, 39 (2020) 336-370.
[6] E.M. McBride, P.M. Mach, E.S. Dhummakupt, S. Dowling, D.O. Carmany, P.S. Demond, G. Rizzo, N.E. Manicke, T. Glaros, Paper spray ionization: Applications and perspectives, TrAC Trends in Analytical Chemistry, 118 (2019) 722-730.
[7] S. Chiang, W. Zhang, Z. Ouyang, Paper spray ionization mass spectrometry: recent advances and clinical applications, Expert Review of Proteomics, 15 (2018) 781-789.
[8] Q. Yang, H. Wang, J.D. Maas, W.J. Chappell, N.E. Manicke, R.G. Cooks, Z. Ouyang, Paper spray ionization devices for direct, biomedical analysis using mass spectrometry, International Journal of Mass Spectrometry, 312 (2012) 201-207.
[9] S. Maher, F.P.M. Jjunju, S. Taylor, Colloquium: 100 years of mass spectrometry: Perspectives and future trends, Reviews of Modern Physics, 87 (2015) 113-135.
[10] N.M. Sarih, D. Romero-Perez, B. Bastani, M. Rauytanapanit, C. Boisdon, T. Praneenararat, H.A. Tajuddin, Z. Abdullah, A.K. Badu-Tawiah, S. Maher, Accelerated nucleophilic substitution reactions of dansyl chloride with aniline under ambient conditions via dual-tip reactive paper spray, Scientific Reports, 10 (2020) 21504.

[11] S. Dowling, E.M. McBride, J. McKenna, T. Glaros, N.E. Manicke, Direct soil analysis by paper spray mass spectrometry: Detection of drugs and chemical warfare agent hydrolysis products, Forensic Chemistry, 17 (2020) 100206.
[12] D.E. Damon, K.M. Davis, C.R. Moreira, P. Capone, R. Cruttenden, A.K. Badu-Tawiah, Direct Biofluid Analysis Using Hydrophobic Paper Spray Mass Spectrometry, Analytical Chemistry, 88 (2016) 1878-1884.
[13] D.E. Damon, Y.S. Maher, M. Yin, F.P.M. Jjunju, I.S. Young, S. Taylor, S. Maher, A.K. Badu-Tawiah, 2D wax-printed paper substrates with extended solvent supply capabilities allow enhanced ion signal in paper spray ionization, Analyst, 141 (2016) 3866-3873.
[14] S. Suraritdechachai, C. Charoenpakdee, I. Young, S. Maher, T. Vilaivan, T. Praneenararat, Rapid Detection of the Antibiotic Sulfamethazine in Pig Body Fluids by Paper Spray Mass Spectrometry, Journal of Agricultural and Food Chemistry, 67 (2019) 3055-3061.
[15] I.W. De Silva, S. Nayek, V. Singh, J. Reddy, J.K. Granger, G.F. Verbeck, Paper spray mass spectrometry utilizing Teslin® substrate for rapid detection of lipid metabolite changes during COVID-19 infection, Analyst, 145 (2020) 5725-5732.
[16] J. McKenna, R. Jett, K. Shanks, N.E. Manicke, Toxicological Drug Screening using Paper Spray High-Resolution Tandem Mass Spectrometry (HR-MS/MS), Journal of analytical toxicology, 42 (2018) 300-310.
[17] Imesha W. De Silva, D.T. Converse, L.A. Juel, G.F. Verbeck, A comparative study of microporous polyolefin silica-based paper and cellulose paper substrates utilizing paper spray-mass spectrometry in drug analysis, Analytical Methods, 11 (2019) 3066-3072.
[18] I. W. De Silva, A.N. Couch, G.F. Verbeck, Paper Spray Mass Spectrometry Utilized with a Synthetic Microporous Polyolefin Silica Matrix Substrate in the Rapid Detection and Identification of More than 190 Synthetic Fentanyl Analogs, Journal of the American Society for Mass Spectrometry, 32 (2021) 420-428.
[19] F.P.M. Jjunju, A. Li, A. Badu-Tawiah, P. Wei, L. Li, Z. Ouyang, I.S. Roqan, R.G. Cooks, In situ analysis of corrosion inhibitors using a portable mass spectrometer with paper spray ionization, Analyst, 138 (2013) 3740-3748.
[20] F.P.M. Jjunju, S. Maher, D.E. Damon, R.M. Barrett, S.U. Syed, R.M.A. Heeren, S. Taylor, A.K. Badu-Tawiah, Screening and Quantification of Aliphatic Primary Alkyl Corrosion Inhibitor Amines in Water Samples by Paper Spray Mass Spectrometry, Analytical Chemistry, 88 (2016) 1391-1400.
[21] S. Maher, F.P.M. Jjunju, D.E. Damon, H. Gorton, Y.S. Maher, S.U. Syed, R.M.A. Heeren, I.S. Young, S. Taylor, A.K. Badu-Tawiah, Direct Analysis and Quantification of Metaldehyde in Water using Reactive Paper Spray Mass Spectrometry, Scientific Reports, 6 (2016) 35643.
[22] F.P.M. Jjunju, D.E. Damon, D. Romero-Perez, I.S. Young, R.J. Ward, A. Marshall, S. Maher, A.K. Badu-Tawiah, Analysis of non-conjugated steroids in water using paper spray mass spectrometry, Scientific Reports, 10 (2020) 10698.
[23] C. Costa, E.M. van Es, P. Sears, J. Bunch, V. Palitsin, H. Cooper, M.J. Bailey, Exploring a route to a selective and sensitive portable system for explosive detection– swab spray ionisation coupled to of high-field assisted waveform ion mobility spectrometry (FAIMS), Forensic Science International: Synergy, 1 (2019) 214-220.
[24] M. Jang, C. Costa, J. Bunch, B. Gibson, M. Ismail, V. Palitsin, R. Webb, M. Hudson, M.J. Bailey, On the relevance of cocaine detection in a fingerprint, Scientific Reports, 10 (2020) 1974.
[25] J. Czerwinska, M. Jang, C. Costa, M.C. Parkin, C. George, A.T. Kicman, M.J. Bailey, P.I. Dargan, V. Abbate, Detection of mephedrone and its metabolites in fingerprints from a controlled human administration study by liquid chromatography-tandem mass spectrometry and paper spray-mass spectrometry, Analyst, 145 (2020) 3038-3048.
[26] C. Costa, M. Ismail, D. Stevenson, B. Gibson, R. Webb, M. Bailey, Distinguishing between Contact and Administration of Heroin from a Single Fingerprint using High Resolution Mass Spectrometry, Journal of analytical toxicology, 44 (2020) 218-225.

[27] R.D. Espy, A.R. Muliadi, Z. Ouyang, R.G. Cooks, Spray mechanism in paper spray ionization, International journal of mass spectrometry, 325 (2012) 167-171.
[28] D. Kim, U.H. Yim, B. Kim, S. Cha, S. Kim, Paper spray chemical ionization: highly sensitive ambient ionization method for low-and nonpolar aromatic compounds, Analytical chemistry, 89 (2017) 9056-9061.
[29] L. Konermann, E. Ahadi, A.D. Rodriguez, S. Vahidi, Unraveling the mechanism of electrospray ionization, in, ACS Publications, 2013.
[30] J.V. Iribarne, B.A. Thomson, On the evaporation of small ions from charged droplets, The Journal of Chemical Physics, 64 (1976) 2287-2294.
[31] M. Dole, L.L. Mack, R.L. Hines, R.C. Mobley, L.D. Ferguson, M.B. Alice, Molecular Beams of Macroions, The Journal of Chemical Physics, 49 (1968) 2240-2249.
[32] L.L. Mack, P. Kralik, A. Rheude, M. Dole, Molecular Beams of Macroions. II, The Journal of Chemical Physics, 52 (1970) 4977-4986.
[33] G. Schmelzeisen-Redeker, L. Bütfering, F.W. Röllgen, Desolvation of ions and molecules in thermospray mass spectrometry, International Journal of Mass Spectrometry and Ion Processes, 90 (1989) 139-150.
[34] L. Konermann, E. Ahadi, A.D. Rodriguez, S. Vahidi, Unraveling the Mechanism of Electrospray Ionization, Analytical Chemistry, 85 (2013) 2-9.
[35] H. Metwally, Q. Duez, L. Konermann, Chain Ejection Model for Electrospray Ionization of Unfolded Proteins: Evidence from Atomistic Simulations and Ion Mobility Spectrometry, Analytical Chemistry, 90 (2018) 10069-10077.
[36] D.E. Damon, Y.S. Maher, D.M. Allen, J. Baker, B.S. Chang, S. Maher, M.M. Thuo, A.K. Badu-Tawiah, Determining Surface Energy of Porous Substrates by Spray Ionization, Langmuir, 35 (2019) 13853-13859.
[37] K.Q.T. A. Gomez, On the structure of an electrostatic spray of monodisperse droplets, Physics of Fluids, 6 ((1994)) 404–414.
[38] I. Marginean, J.S. Page, A.V. Tolmachev, K. Tang, R.D. Smith, Achieving 50% Ionization Efficiency in Subambient Pressure Ionization with Nanoelectrospray, Analytical Chemistry, 82 (2010) 9344-9349.
[39] R.T.K. J. S. Page, K. Tang, R. D. Smith, Ionization and transmission efficiency in an electrospray ionization-mass spectrometry interface, Journal of American Society of Mass Spectrometry, 18 (2007) 1582–1590.
[40] M. Pauly, M. Sroka, J. Reiss, G. Rinke, A. Albarghash, R. Vogelgesang, H. Hahne, B. Kuster, J. Sesterhenn, K. Kern, A hydrodynamically optimized nano-electrospray ionization source and vacuum interface, Analyst, 139 (2014) 1856-1867.
[41] J.S. Page, R.T. Kelly, K. Tang, R.D. Smith, Ionization and transmission efficiency in an electrospray ionization—mass spectrometry interface, Journal of the American Society for Mass Spectrometry, 18 (2007) 1582-1590.
[42] I. Manisali, D.D.Y. Chen, B.B. Schneider, Electrospray ionization source geometry for mass spectrometry: past, present, and future, TrAC Trends in Analytical Chemistry, 25 (2006) 243-256.
[43] J. Murphy, J. Johnson, P. Rainville, Enhancing Mass Spectrometry Sensitivity by Reducing Chromatographic Flow Rates with ionKey/MS, in, 2014.
[44] K.L. Davidson, D.R. Oberreit, C.J. Hogan, M.F. Bush, Nonspecific aggregation in native electrokinetic nanoelectrospray ionization, International Journal of Mass Spectrometry, 420 (2017) 35-42.
[45] R. Juraschek, T. Dülcks, M. Karas, Nanoelectrospray—more than just a minimized-flow electrospray ionization source, Journal of the American Society for Mass Spectrometry, 10 (1999) 300-308.
[46] S.K. Chowdhury, V. Katta, B.T. Chait, An electrospray-ionization mass spectrometer with new features, Rapid Communications in Mass Spectrometry, 4 (1990) 81-87.
[47] D.A.C. L. Y. T. Li, P. K. Bennett, J. Henion, Acceptance criteria for ultra trace HPLC – tandem mass spectrometry, Analytical Chemistry, 68 (1996) 3397.

[48] R.A.B. J. P. Allanson, A. E. Jones, S. Pleasance, The use of automated SPE in the '96 well' format for high throughput bioanalysis using LC-MS-MS, Rapid Comm. Mass Spec., 10 (1996) 811.
[49] H.L. R. D. Voyksner, Improvements in LC/Electrospray Ion Trap Mass Spectrometry Performance Using an Off-Axis Nebulizer, Analytical Chemistry, 71 (1999) 1441-1447.
[50] R.M. T. Bantan, B. Mitrovic, B. Pihlar, Investigation of low molecular weight Al complexes in human serum by fast protein liquid chromatography (FPLC)-ETAAS and electrospray (ES)-MS-MS techniques, J. Anal. At. Spectrom., 14 (1999) 1743-1748.
[51] B.B. Schneider, D.J. Douglas, D.D.Y. Chen, An atmospheric pressure ion lens that improves nebulizer assisted electrospray ion sources, Journal of the American Society for Mass Spectrometry, 13 (2002) 906-913.
[52] P.A. Kottke, J.Y. Lee, A.P. Jonke, C.A. Seneviratne, E.S. Hecht, D.C. Muddiman, M.P. Torres, A.G. Fedorov, DRILL: An Electrospray Ionization-Mass Spectrometry Interface for Improved Sensitivity via Inertial Droplet Sorting and Electrohydrodynamic Focusing in a Swirling Flow, Analytical Chemistry, 89 (2017) 8981-8987.
[53] C.L. Feider, A. Krieger, R.J. DeHoog, L.S. Eberlin, Ambient Ionization Mass Spectrometry: Recent Developments and Applications, Analytical Chemistry, 91 (2019) 4266-4290.
[54] J. Liu, H. Wang, N.E. Manicke, J.-M. Lin, R.G. Cooks, Z. Ouyang, Development, Characterization, and Application of Paper Spray Ionization, Analytical Chemistry, 82 (2010) 2463-2471.
[55] L. Shen, J. Zhang, Q. Yang, N.E. Manicke, Z. Ouyang, High throughput paper spray mass spectrometry analysis, Clinica Chimica Acta, 420 (2013) 28-33.
[56] C. Zhang, N.E. Manicke, Development of a paper spray mass spectrometry cartridge with integrated solid phase extraction for bioanalysis, Analytical chemistry, 87 (2015) 6212-6219.
[57] G.I. Salentijn, R.D. Oleschuk, E. Verpoorte, 3D-Printed Paper Spray Ionization Cartridge with Integrated Desolvation Feature and Ion Optics, Analytical Chemistry, 89 (2017) 11419-11426.
[58] G.I. Salentijn, H.P. Permentier, E. Verpoorte, 3D-printed paper spray ionization cartridge with fast wetting and continuous solvent supply features, Analytical chemistry, 86 (2014) 11657-11665.
[59] A.D. Appelhans, D.A. Dahl, SIMION ion optics simulations at atmospheric pressure, International Journal of Mass Spectrometry, 244 (2005) 1-14.
[60] C. Baumgärtel, R.T. Smith, S. Maher, Accurately predicting electron beam deflections in fringing fields of a solenoid, Scientific Reports, 10 (2020) 10903.
[61] R.T. Smith, F.P. Jjunju, S. Maher, Evaluation of electron beam deflections across a solenoid using Weber-Ritz and Maxwell-Lorentz electrodynamics, Progress In Electromagnetics Research, 151 (2015) 83-93.
[62] R.T. Smith, F.P.M. Jjunju, I.S. Young, S. Taylor, S. Maher, A physical model for low-frequency electromagnetic induction in the near field based on direct interaction between transmitter and receiver electrons, Proceedings of the Royal Society A: Mathematical, Physical and Engineering Sciences, 472 (2016) 20160338.
[63] B.L. Smith, N.A. Smith, F.P. Jjunju, I.S. Young, J. Vossebeld, G. Casse, S. Taylor, S. Maher, 50-Channel charge integrating faraday detector for characterization of ambient ions, in: 2017 IEEE SENSORS, 2017, pp. 1-3.
[64] M. Schulz, S. Iwersen-Bergmann, H. Andresen, A. Schmoldt, Therapeutic and toxic blood concentrations of nearly 1,000 drugs and other xenobiotics, Critical Care, 16 (2012) R136.
[65] U. FDA, Guidance for Industry: Bioanalytical Method Validation,(Draft Guidance), US FDA, (2013).
[66] R.M. Bain, C.J. Pulliam, S.T. Ayrton, K. Bain, R.G. Cooks, Accelerated hydrazone formation in charged microdroplets, Rapid Commun. Mass Spectrom., 30 (2016) 1875-1878.

Acknowledgments

S.M. and B.L.S. are very grateful for the support received from EPSRC (EP/V001019/1). S.M., S.Mc. and T-T.S. acknowledge support from Alder Hey Children's Hospital Kidney Research Fund.